Published October 18, 2004

Defective function of GABA-containing synaptic vesicles in mice lacking the AP-3B clathrin adaptor

Fubito Nakatsu,[1,2] Motohiro Okada,[3] Fumiaki Mori,[4] Noriko Kumazawa,[5] Hiroto Iwasa,[3] Gang Zhu,[3] Yasufumi Kasagi,[6] Haruyuki Kamiya,[8] Akihiro Harada,[9] Kazuhiro Nishimura,[10] Arata Takeuchi,[1,7] Taisuke Miyazaki,[11] Masahiko Watanabe,[11] Shigeki Yuasa,[12] Toshiya Manabe,[5] Koichi Wakabayashi,[4] Sunao Kaneko,[3] Takashi Saito,[1,7] and Hiroshi Ohno[1,2]

[1]RIKEN Research Center for Allergy and Immunology, Kanagawa 230-0045, Japan
[2]Division of Molecular Membrane Biology, Cancer Research Institute, Kanazawa University, Kanazawa 920-0934, Japan
[3]Department of Neuropsychiatry, Hirosaki University School of Medicine, Hirosaki 036-8216, Japan
[4]Department of Neuropathology, Institute of Brain Science, Hirosaki University School of Medicine, Hirosaki 036-8562, Japan
[5]Division of Neuronal Network, Department of Basic Medical Sciences, Institute of Medical Science, University of Tokyo, Tokyo 108-8639, Japan
[6]Department of Integrative Neurophysiology and [7]Department of Molecular Genetics, Chiba University Graduate School of Medicine, Chiba 260-8670, Japan
[8]Division of Cell Biology and Neurophysiology, Department of Neuroscience, Faculty of Medicine, Kobe University, Kobe 650-0017, Japan
[9]Laboratory of Cellular and Molecular Morphology, Department of Cell Biology, Institute for Molecular and Cellular Regulation, Gunma University, Gunma 371-8512, Japan
[10]Department of Clinical Biochemistry, Graduate School of Pharmaceutical Sciences, Chiba University, Chiba 260-8675, Japan
[11]Department of Anatomy, Hokkaido University School of Medicine, Sapporo 060-8638, Japan
[12]Department of Ultrastructural Research, National Institute of Neuroscience, Tokyo 187-8502, Japan

AP-3 is a member of the adaptor protein (AP) complex family that regulates the vesicular transport of cargo proteins in the secretory and endocytic pathways. There are two isoforms of AP-3: the ubiquitously expressed AP-3A and the neuron-specific AP-3B. Although the physiological role of AP-3A has recently been elucidated, that of AP-3B remains unsolved. To address this question, we generated mice lacking μ3B, a subunit of AP-3B. μ3B$^{-/-}$ mice suffered from spontaneous epileptic seizures. Morphological abnormalities were observed at synapses in these mice. Biochemical studies demonstrated the impairment of γ-aminobutyric acid (GABA) release because of, at least in part, the reduction of vesicular GABA transporter in μ3B$^{-/-}$ mice. This facilitated the induction of long-term potentiation in the hippocampus and the abnormal propagation of neuronal excitability via the temporoammonic pathway. Thus, AP-3B plays a critical role in the normal formation and function of a subset of synaptic vesicles. This work adds a new aspect to the pathogenesis of epilepsy.

Introduction

Adaptor protein (AP) complexes, along with clathrin, regulate the formation of clathrin-coated vesicles and the signal-mediated sorting of integral membrane proteins in the late secretory and endocytic pathways (Nakatsu and Ohno, 2003). AP complexes consist of four subunits, including two large chains (α, γ, δ or ε and β), one medium chain (μ), and one small chain (σ) (Hirst and Robinson, 1998; Bonifacino and Dell'Angelica, 1999). We have demonstrated previously that μ subunits directly recognize tyrosine-based sorting motifs, one of the most commonly used sorting signals within the cytoplasmic tail of cargo membrane proteins, which enables the signal-mediated vesicular transport (Ohno et al., 1995; Kirchhausen et al., 1997). Six distinct μ subunits exist in mammalian genome (Boehm and Bonifacino, 2001). Among them are the two isoforms of μ3, μ3A, and μ3B. μ3A is ubiquitously expressed and forms the AP-3A complex in conjunction with, δβ3A, and σ3 subunits. AP-3A plays an important role in the transport of membrane proteins to, as well as the biogenesis of, lysosomes and lysosome-related organelles (Odorizzi et al., 1998). In contrast, μ3B is exclusively expressed in neurons and forms the neuron-specific AP-3B complex along with β3B, another neuron-specific subunit (Pevsner et al., 1994; Newman et al., 1995). The other two subunits of AP-3B, δ, and σ3, are shared by the two AP-3 isoforms.

Mutations in the β3A subunit of ubiquitous AP-3A have been identified in patients suffering from the Hermansky-Pudlak syndrome (HPS), in which the function and/or biogenesis of lysosomes and lysosome-related organelles such as melano-

F. Nakatsu, M. Okada, and F. Mori contributed equally to this work.

The online version of this article contains supplemental material.

Correspondence to Hiroshi Ohno: ohno@rcai.riken.jp

Abbreviations used in this paper: AP, adaptor protein; EC, entorhinal cortex; ES, embryonic stem; GABA, γ-aminobutyric acid; HPS, Hermansky-Pudlak syndrome; LTP, long-term potentiation; Neo, neomycin; PTX, picrotoxin; PTZ, pentylenetetrazole; TA, temporoammonic; VGAT, vesicular GABA transporter.

Supplemental Material can be found at:
http://jcb.rupress.org/content/suppl/2004/10/18/jcb.200405032.DC1.html

The Journal of Cell Biology, Vol. 167, No. 2, October 25, 2004 293–302
http://www.jcb.org/cgi/doi/10.1083/jcb.200405032

Published October 18, 2004

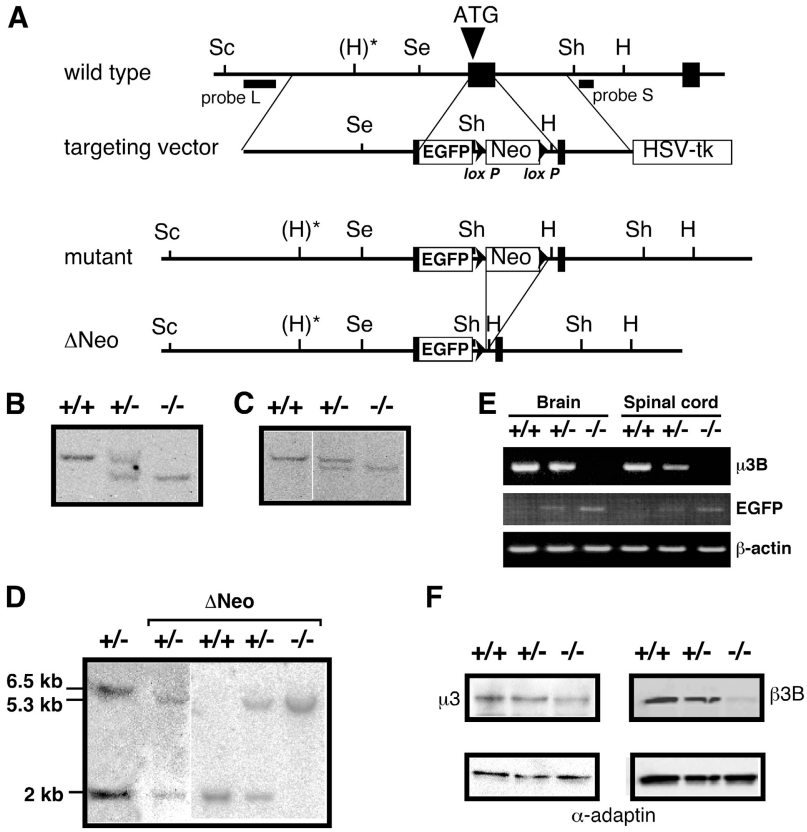

Figure 1. **Targeted disruption of μ3B gene by homologous recombination.** (A) Structure of mouse μ3B gene including the exon encoding ATG start codon (wild type); the targeting vector containing 5′ (3.0 kb) and 3′ (1.5 kb) homologous regions, the EGFP gene, the Neo gene flanked with two loxP sites, and the herpes simplex virus-thymidine kinase (HSV-*tk*) gene for positive and negative selections (targeting vector); the resultant mutant allele generated by homologous recombination (mutant); and the mutant allele lacking the Neo gene after crossing with Cre-transgenic mice (ΔNeo). The following restriction enzyme sites are indicated: H, HindIII; Sc, SacI; Se, SpeI; and Sh, SphI. An additional HindIII site, shown by (H)*, exists only in the genome from C57BL/6 mice and not in that from 129 mice. (B–D) Southern blotting using 5′ (probe L) and 3′ (probe S) probes as depicted in A. Digestion of genome DNA with HindIII and SpeI yielded a 3.6-kb wild-type band and a 2.5-kb band generated by homologous recombination using probe S (B). Similarly, digestion of genome DNA with SacI and SphI yielded a 6.4-kb wild-type band and a 5.5-kb band generated by homologous recombination using probe L (C). The mutant allele digested with HindIII and SacI became 1.2 kb shorter (from 6.5 to 5.3 kb) using probe L after deletion of the Neo gene by crossing with Cre-transgenic mice (D, compare first and second lanes). Data shown in D were obtained using mice with C57BL/6 background. Note that the additional HindIII site ((H)*, A) in C57BL/6 genome gave a 2-kb band corresponding the C57BL/6 wild-type allele (third lane). (E) RT-PCR analysis using total RNA from brain (left) or spinal cord (right) as a template for PCR. (F) Whole brain lysates from wild-type, $\mu3B^{+/-}\Delta$Neo and $\mu3B^{-/-}\Delta$Neo mice were subjected to immunoblotting with anti-μ3 (top left) and anti-β3B (top right) antibodies. After stripping off the antibodies, both membranes were reblotted with anti–α adaptin (bottom) as an internal control for the amount of protein in each lane.

somes and platelet dense granules are impaired (Dell'Angelica et al., 1999; Swank et al., 2000). As a result, the HPS patients suffer from such symptoms as abnormal secretion of lysosomal enzymes, pigmentation defect, and prolonged bleeding time. *Pearl* mice, one of the HPS model mutants, also bear a mutation in the β3A gene and share the same phenotypes with HPS patients (Feng et al., 1999). Another HPS model, *mocha* mice, has mutations in the common δ subunit (Kantheti et al., 1998). As a result, in addition to the phenotypes seen in *pearl* mice and HPS patients, *mocha* mice suffer from neurological disorders, such as abnormal electrocorticogram, the recording of electrical activity from cerebral cortex, and inner ear disorders (deafness and balance problem; Rolfsen and Erway, 1984; Noebels and Sidman, 1989; Kantheti et al., 1998). It is possible that these dysfunctions are due to the absence of AP-3B in *mocha* mice, although little is known about the role of AP-3B in vivo.

To investigate the physiological role of AP-3B, we generated μ3B-deficient mice using the gene targeting technique. Morphological analyses indicated that AP-3B is involved in the biogenesis of synaptic vesicles in vivo. Biochemical and electrophysiological studies corroborated the dysfunction of γ-aminobutyric acid (GABA) ergic synaptic transmission in $\mu3B^{-/-}$ mice. Consequently, the $\mu3B^{-/-}$ mice suffered from spontaneous recurrent epileptic seizures. These findings suggest that AP-3B is responsible for efficient synaptic transmission, particularly the inhibitory one, by regulating the formation and function of a subset of synaptic vesicles.

Results

Generation of μ3B-deficient mice

To disrupt the μ3B locus in E14.1 embryonic stem (ES) cells, the downstream of the start codon of μ3B exon 2 was replaced with EGFP cDNA and neomycin (Neo) resistance gene flanked with loxP sequences by homologous recombination (Fig. 1 A). ES cell lines with the mutant allele were injected into blastocysts from C57BL/6 mice to obtain chimeric offspring. After crossing these chimeras with C57BL/6 mice, heterozygous animals were identified by Southern blotting of tail DNA using 5′ and 3′ probes (Fig. 1, B and C). It has been reported that Neo gene inserted into the genome may perturb the expression of adjacent genes in several knockout mice (Olson et al., 1996). To avoid this possibility, we removed Neo gene by crossing the $\mu3B^{-/-}$ mice with Cre-transgenic mice (Sakai and Miyazaki, 1997) to establish $\mu3B^{-/-}\Delta$Neo mice (Fig. 1 D). We further backcrossed $\mu3B^{-/-}\Delta$Neo mice with C57BL/6 mice to avoid a possible variation of the phenotype(s) with the mixed genotype of C57BL/6 × 129.

The disruption of the μ3B gene in $\mu3B^{-/-}\Delta$Neo mice was verified by RT-PCR (Fig. 1 E). The expression of μ3B transcripts was detected in the brain and the spinal cord of wild-type and $\mu3B^{+/-}\Delta$Neo mice, but not in those of $\mu3B^{-/-}\Delta$Neo mice. Alternatively, EGFP gene was expressed only in $\mu3B^{+/-}\Delta$Neo and $\mu3B^{-/-}\Delta$Neo mice. We also detected the expression of EGFP immunohistochemically in neurons

Published October 18, 2004

throughout the brain, with stronger signals particularly in the hippocampus and the dentate gyrus (unpublished data), where β3B, another neuron-specific subunit of AP-3B, was also abundantly expressed (Newman et al., 1995). Immunoblot analysis of μ3A/B using anti-μ3A/B antibody revealed that the amount of μ3 proteins in whole brain lysates from μ3B$^{-/-}$ΔNeo mice was decreased to approximately half that from wild-type mice, indicating that there is no compensatory mechanism for μ3B deficiency by increasing the amount of μ3A protein in μ3B$^{-/-}$ΔNeo mice (Fig. 1 F). Immunoblot analysis also revealed that the expression of β3B, another neuron-specific subunit of AP-3B, was barely detectable in μ3B$^{-/-}$ΔNeo mice (Fig. 1 F), consistent with previous studies (Kantheti et al., 1998; Dell'Angelica et al., 1999) showing that other subunits of AP complexes become unstable and are rapidly degraded in the absence of one of their subunits, and indicating that β3B can assemble with only μ3B and not μ3A to constitute the neuron-specific AP-3B. Thus, the disruption of μ3B resulted in the disappearance of AP-3B in μ3B$^{-/-}$ΔNeo mice.

Seizure susceptibility of μ3B$^{-/-}$ΔNeo mice

The frequency of birth of μ3B$^{-/-}$ΔNeo mice was in accordance with Mendelian expectations. The mice were fertile and survived for at least more than one year. Although the μ3B$^{-/-}$ΔNeo mice appeared normal, some adult mice exhibited spontaneous epileptic seizures upon presentation of such stimuli as positional change (Video 1, available at http://www.jcb.org/cgi/content/full/jcb.200405032/DC1). More than half of the mice suffered from seizures at the age of 15 wk or over. In addition, the electrocorticogram revealed that all of the μ3B$^{-/-}$ΔNeo mice tested showed an abnormal epileptic pattern, namely, interictal spikes, which was never observed in wild-type mice (Fig. 2 A). These observations prompted us to test the seizure susceptibility of μ3B$^{-/-}$ΔNeo mice.

Intravenous infusion of pentylenetetrazole (PTZ), a $GABA_A$ receptor antagonist, elicits a series of stereotyped responses beginning with a period of intermittent twitches of the head and body, leading to tonic–clonic activity, followed by a phase of tonic extension and death (Tecott et al., 1995). PTZ was infused into the tail vein of wild-type and μ3B$^{-/-}$ΔNeo mice, and the susceptibility to PTZ was analyzed. Both 4- and 8-wk-old μ3B$^{-/-}$ΔNeo mice required only 40–70% of the amount of PTZ required by wild-type mice to reach the same stages of seizure (Fig. 2 B).

We further examined the seizure susceptibility of μ3B$^{-/-}$ΔNeo mice by electrical kindling, an established model for experimental seizure (Goddard, 1967). Generalized seizure (class 5) was observed in wild-type mice after 10–12 stimulations (Fig. 2 C). Notably, all the μ3B$^{-/-}$ΔNeo mice tested reached class 5 within the first two stimulations. Consistently, the afterdischarge, electrical activity recorded after stimulation, evoked by the first kindling stimulation lasted much longer in μ3B$^{-/-}$ΔNeo mice than in wild-type mice (Fig. 2 D; average of the duration of afterdischarge: 7.0 ± 1.3 s in wild-type mice (n = 4) vs. 14.1 ± 4.1 s in μ3B$^{-/-}$ΔNeo mice (n = 4), $P < 0.05$, t test). Furthermore,

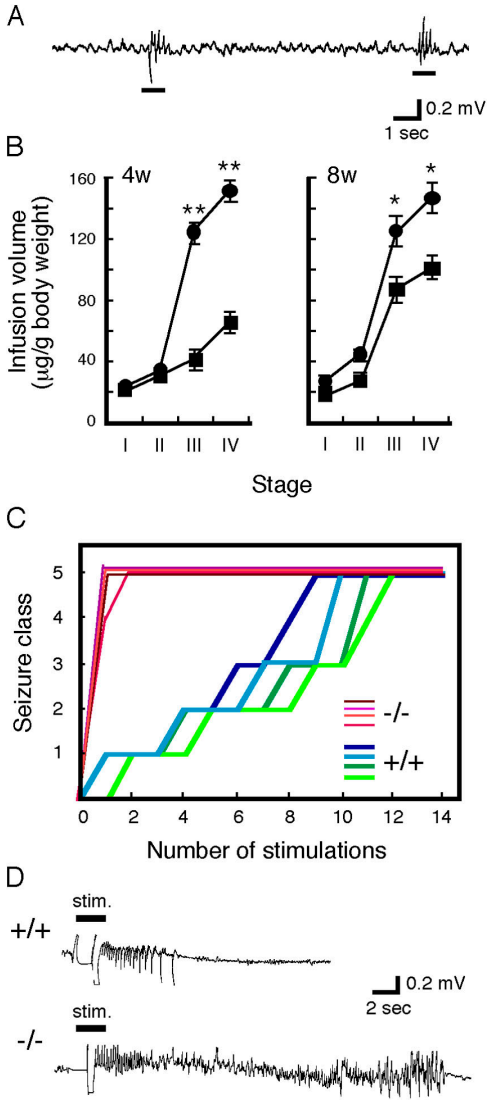

Figure 2. **Increased seizure susceptibility of μ3B$^{-/-}$ΔNeo mice.** (A) Representative electrocorticogram recorded from μ3B$^{-/-}$ΔNeo mice (n = 7) during the interictal period. Interictal spikes are underlined. (B) Seizure was induced by intravenous administration of PTZ, a $GABA_A$ receptor antagonist, in 4-wk-old (left) and 8-wk-old (right) wild-type (closed circle; 4 wk old, n = 6; 8 wk old, n = 5) and μ3B$^{-/-}$ΔNeo (closed square; 4 wk old, n = 4; 8 wk old, n = 5) mice. Seizure stages were judged as described previously (see Materials and methods). Results are expressed as means ± SEM (* indicates $P < 0.05$; ** indicates $P < 0.01$). (C) Seizure development by amygdala kindling. Kindling experiments were performed as described previously (see Materials and methods), and the development of seizure classes in individual animals is plotted against the number of kindling stimulations. (D) Typical afterdischarge of wild-type (top) or μ3B$^{-/-}$ΔNeo mice (bottom) induced by the first kindling stimulation.

the seizure phenotype of μ3B$^{-/-}$ΔNeo mice subjected to kindling stimulation was different from that of wild-type mice, but identical to the spontaneous seizure displayed by μ3B$^{-/-}$ΔNeo mice (unpublished data). Therefore, it is likely that the generalized seizure in μ3B$^{-/-}$ΔNeo mice evoked by kindling stimulation is due to intrinsic epileptogenesis rather than acquired one by the kindling. Together, these results demonstrate that μ3B$^{-/-}$ΔNeo mice have higher seizure susceptibility than wild-type mice.

Published October 18, 2004

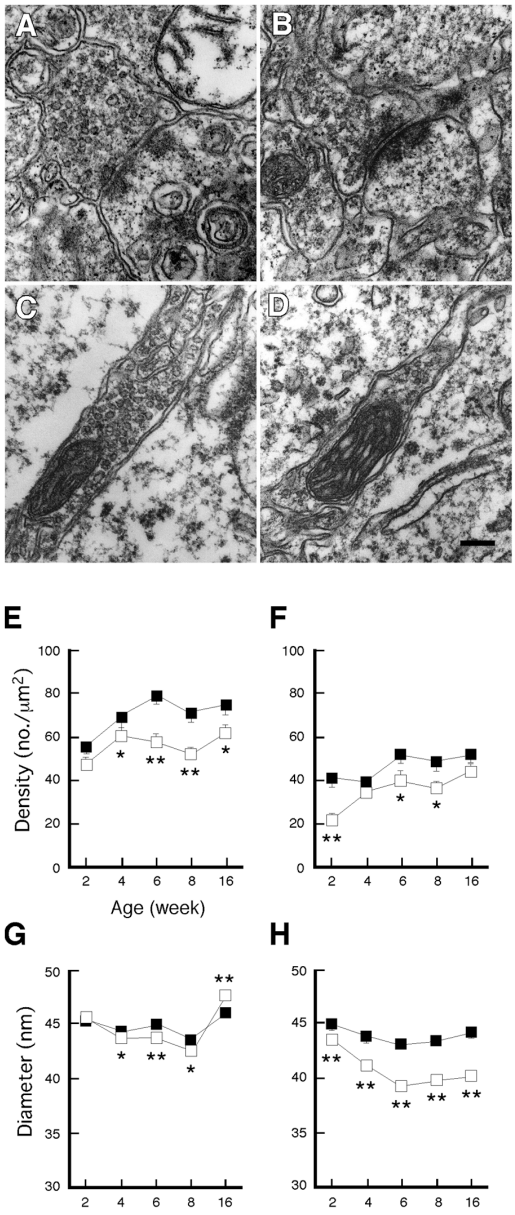

Figure 3. **Ultrastructural analysis of synaptic terminals.** (A–D) Electron micrographs of asymmetric (excitatory) terminals (A and B) and symmetric (inhibitory) terminals attaching to perikarya of CA1 pyramidal neurons (C and D) in the CA1 in wild-type (A and C) and μ3B$^{-/-}$ΔNeo (B and D) mice at the age of 8 wk. Bar, 200 nm. (E–H) Developmental changes in the number of synaptic vesicles per unit area (E and F) and the diameter of synaptic vesicles (G and H) of excitatory (E and G) and inhibitory terminals (F and H) in μ3B$^{-/-}$ΔNeo mice (open square) and wild-type mice (solid square). 30–50 areas (E and F) and >500 synaptic vesicles (G and H) from both genotypes ($n = 3$ each) were counted, respectively. Values are expressed as means ± SEM Student's or Welch's *t* test was used to determine the differences between μ3B$^{-/-}$ΔNeo and wild-type mice (* indicates $P < 0.05$; ** indicates $P < 0.01$).

Morphological abnormalities in excitatory and inhibitory presynaptic terminals of μ3B$^{-/-}$ΔNeo mice

There was no difference in brain weight between wild-type and μ3B$^{-/-}$ΔNeo mice at any of the postnatal developmental phases. Conventional histological examination including Nissl as well as hematoxylin and eosin staining revealed no abnormality in the overall structure of the brain from μ3B$^{-/-}$ΔNeo mice (unpublished data). Immunohistochemistry showed no astrogliosis in the hippocampus, indicative of neuronal degeneration, suggesting that apparent neuronal cell death does not occur in μ3B$^{-/-}$ΔNeo mice (unpublished data).

We next performed ultrastructural examination of the hippocampus. The number of synaptic vesicles per unit area was decreased in μ3B$^{-/-}$ΔNeo mice. The density of synaptic vesicles in excitatory terminals was lower in μ3B$^{-/-}$ΔNeo mice than in wild-type mice at the age of 4–16 wk (Fig. 3, A, B, and E). The density of synaptic vesicles in inhibitory terminals was also lower in μ3B$^{-/-}$ΔNeo mice than in wild-type mice at the age of 2, 6, and 8 wk (Fig. 3, C, D, and F). In addition, the diameter of the synaptic vesicles in inhibitory synaptic terminals in μ3B$^{-/-}$ΔNeo mice was evidently smaller than that in wild-type mice (Fig. 3, G and H). Thus, these results indicate that AP-3B is involved in the biogenesis of synaptic vesicles in hippocampus in vivo.

Impairment of GABA release due to reduction of VGAT in μ3B$^{-/-}$ΔNeo mice

That μ3B$^{-/-}$ΔNeo mice exhibited morphological abnormalities in synapses led us to ask whether the release of neurotransmitters was impaired in these mice. To this end, the release of glutamate and GABA in the hippocampal minislice was measured. The amounts of basal release were similar between μ3B$^{-/-}$ΔNeo mice and wild-type mice at all the ages tested (Fig. 4, A and B). However, the K^+-evoked release of GABA, but not of glutamate, was impaired in μ3B$^{-/-}$ΔNeo mice at 8 wk old or over (Fig. 4, A and B). As the contents of these neurotransmitters in the hippocampus were equivalent between wild-type and μ3B$^{-/-}$ΔNeo mice (unpublished data), the difference in GABA release could not be attributed to the changes in the metabolism of GABA itself. Therefore, we postulated that the accumulation of GABA in synaptic vesicles may be impaired, and examined the amounts of vesicular GABA transporter (VGAT) and VGLUT, transporters responsible for the uptake of GABA and glutamate into the synaptic vesicles, respectively (McIntire et al., 1997; Reimer et al., 1998; Gasnier, 2000; Fremeau et al., 2001). The amount of VGAT protein was decreased significantly in synaptosomal lysates from the hippocampus of μ3B$^{-/-}$ΔNeo mice (Fig. 4, C and D) despite the fact that the amounts of VGLUT1 and VGLUT2, and other synaptic vesicle proteins such as synaptophysin, synaptotagmin, VAMP2, rabphilin-3A, and Rab3A (Fig. 4 C) were unchanged. This was not due to the decrease or loss of the inhibitory neurons themselves, because there was no difference in the number of neurons immunoreactive for GAD67, a marker for inhibitory neurons (unpublished data). These results suggest that the impairment of GABA release in μ3B$^{-/-}$ΔNeo mice is attributable, at least in part, to the decrease in the amount of VGAT protein in the hippocampus.

As we mentioned earlier, μ3B is expressed in neurons throughout the brain despite strongest in hippocampus. To test whether the reduction of VGAT proteins is limited to the hippocampus, we performed biochemical quantification of the

Published October 18, 2004

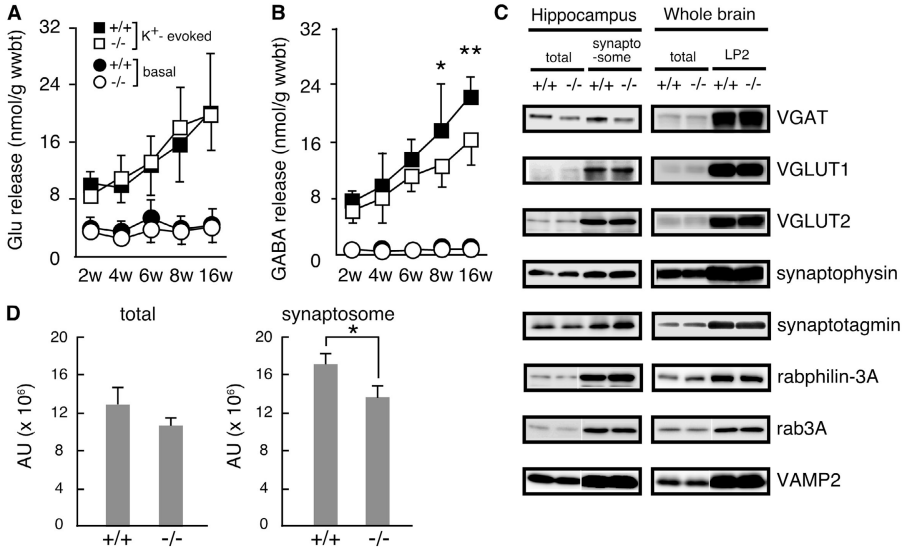

Figure 4. **Impairment of GABA release due to reduction of VGAT in μ3B$^{-/-}$ΔNeo mice.** (A and B) Measurement of glutamate (A) and GABA (B) release was performed as described in Materials and methods. Basal (circles) and K^+-evoked (squares) release of wild-type (closed symbols) and μ3B$^{-/-}$ΔNeo mice (open symbols) is shown ($n = 3$ each). Results are expressed as means ± SEM (* indicates $P < 0.05$; ** indicates $P < 0.01$). (C) Western blotting of VGAT, VGLUT1, VGLUT2, synaptophysin, synaptotagmin, rabphilin-3A, Rab3A, and VAMP2 in total (lanes 1, 2, 5, and 6) and synaptosomal (lanes 3 and 4) or LP2 (lanes 7 and 8) lysates from hippocampus (left) and whole brain (right) of wild-type (lanes 1, 3, 5, and 7) and μ3B$^{-/-}$ΔNeo (lanes 2, 4, 6, and 8) mice. Shown are the representatives of four independent experiments. (D) Quantitative analysis of the amount of VGAT protein in total (left) and synaptosomal (right) hippocampal lysates of wild-type and μ3B$^{-/-}$ΔNeo mice ($n = 4$ each) as shown in C. Results are expressed as means ± SD. (* indicates $P < 0.05$). AU, arbitrary unit.

VGAT protein level in the whole brain. In contrast to the hippocampus, the amount of VGAT, along with other synaptic vesicle proteins, in the crude synaptic vesicle fraction LP2 as well as in the total lysate from μ3B$^{-/-}$ΔNeo whole brain was equivalent to those from wild-type whole brain (Fig. 4 C), suggesting that AP-3B is involved in the biogenesis of a subset of synaptic vesicles in vivo.

We next examined whether μ3B deficiency affected the localization of the synaptic vesicle proteins including VGAT. Immunohistochemical staining revealed that the distribution of VGAT in the hippocampus from μ3B$^{-/-}$ΔNeo mice is comparable to that from wild-type mice (Fig. S1, A and I, available at http://www.jcb.org/cgi/content/full/jcb.200405032/DC1). In cultured hippocampal neurons, VGAT was observed only in axon, where it colocalized with synaptophysin in μ3B-deficient as well as wild-type neurons at 3 d in vitro (Fig. S1, B and J), suggesting that VGAT was targeted to the axon properly in μ3B-deficient neuron. At 14 d in vitro, VGAT was colocalized with both synaptophysin (Fig. S1, C, D, K, and L) and synaptotagmin (Fig. S1, G and O) at synaptic boutons in wild-type and μ3B$^{-/-}$ΔNeo neurons. VGLUT1 was also colocalized with both synaptophysin (Fig. S1, E, F, M, and N) and synaptotagmin (not depicted) in neurons from both genotypes. Localization of VAMP2 was also normal in μ3B$^{-/-}$ΔNeo neuron (Fig. S1, H and P). These results indicate that there is no obvious abnormality in the localization of synaptic vesicle proteins including VGAT in μ3B$^{-/-}$ΔNeo neurons.

Synaptic potentiation is enhanced in μ3B$^{-/-}$ΔNeo mice through reduced GABAergic synaptic inhibition

It is well established that the threshold for the induction of long-term potentiation (LTP) of excitatory synaptic transmission in the hippocampal CA1 region is regulated by $GABA_A$ receptor-mediated inhibitory synaptic inputs that are activated by afferent fiber stimulation for LTP induction (Wigstrom and Gustafsson, 1983): disinhibition by the blockade of $GABA_A$ receptor facilitates LTP induction. To test whether GABAergic synaptic inhibition is impaired in μ3B$^{-/-}$ΔNeo mice, we examined the effect of picrotoxin (PTX; 100 μM), a $GABA_A$ receptor antagonist, on LTP induction. LTP induced by standard conditioning (100 Hz for 1 s) in μ3B$^{-/-}$ΔNeo mice was intact either in the presence ($P > 0.05$; Fig. 5 A) or in the absence ($P > 0.05$; Fig. 5 B) of PTX. However, when weak conditioning (100 Hz for 200 ms) was applied in the absence of PTX (Fig. 5 D), LTP was not induced in wild-type mice (99.3 ± 1.4% of baseline), whereas stable potentiation was induced in μ3B$^{-/-}$ΔNeo mice (117.7 ± 1.7% of baseline; $P < 0.05$). This difference disappeared when PTX was present ($P > 0.05$; Fig. 5 C), indicating that the phenotype observed in Fig. 5 D was dependent on $GABA_A$ receptor-mediated synaptic transmission. Thus, it is conceivable that when a weaker tetanus is used, the influence of inhibition is relatively stronger and LTP induction is suppressed in wild-type mice, whereas LTP is induced in μ3B$^{-/-}$ΔNeo mice because the inhibition is weaker. These results suggest impaired GABAergic synaptic transmission in μ3B$^{-/-}$ΔNeo mice, and are consistent with the reduced GABA release from presynaptic terminals in μ3B$^{-/-}$ΔNeo mice.

Abnormal propagation of neuronal excitability to CA1 pyramidal cell via TA pathway in μ3B$^{-/-}$ΔNeo mice

To investigate the influence of the impairment in GABAergic synapses on hippocampal transmission in μ3B$^{-/-}$ΔNeo mice, we analyzed the propagation of neuronal excitability from the entorhinal cortex (EC) to the hippocampus using optical recording. It is well established that superficial layers of the EC project to the dentate gyrus granule cells via the perforant pathway, and to CA1 pyramidal cells via the temporoammonic (TA) pathway (Heinemann et al., 2000). The TA pathway is composed of both direct excitatory and indirect inhibitory GABAergic interneuron-associated projections (Fig. 6 A; Hei-

Published October 18, 2004

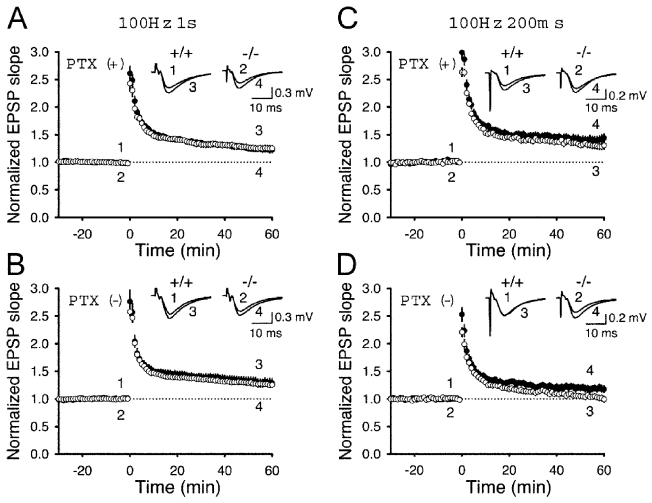

Figure 5. **Enhanced synaptic potentiation through reduced GABAergic synaptic inhibition in μ3B$^{-/-}$ΔNeo mice.** (A–D) The average time course of the slope of synaptic responses in μ3B$^{-/-}$ΔNeo mice and their littermate wild-type mice. Initial EPSP slopes were normalized in each experiment to the average slope value of the baseline (−30–0 min). The potentiation ratio was calculated by dividing the average slope value from 50 to 60 min by that of the baseline. Afferent fibers were tetanized at time 0 at: (A) 100 Hz for 1 s in the presence of PTX in wild-type (open circles; $n = 18$) and μ3B$^{-/-}$ΔNeo (closed circles; $n = 19$) mice; (B) 100 Hz for 1 s in the absence of PTX in wild-type (open circles; $n = 16$) and μ3B$^{-/-}$ΔNeo (closed circles; $n = 13$) mice; (C) 100 Hz for 200 ms in the presence of PTX in wild-type (open circles; $n = 10$) and μ3B$^{-/-}$ΔNeo (closed circles; $n = 10$) mice; and (D) 100 Hz for 200 ms in the absence of PTX in wild-type (open circles; $n = 14$) and μ3B$^{-/-}$ΔNeo (closed circles; $n = 15$) mice.

nemann et al., 2000; Remondes and Schuman, 2002). In 4-wk-old wild-type and μ3B$^{-/-}$ΔNeo mice as well as in 8-wk-old wild-type mice, the neuronal excitability evoked by electrical stimulation of layers II, III, and IV in EC propagated to the dentate gyrus via the perforant pathway, but not to the CA1 pyramidal cells via the TA pathway (Fig. 6, B and C). In contrast, the neuronal excitability propagated from EC to CA1 pyramidal cells in addition to the dentate gyrus in 8-wk-old μ3B$^{-/-}$ΔNeo mice (Fig. 6, B and C). Consistent with our previous observation (Okada et al., 2004), the propagation of neuronal excitability via both perforant and TA pathways was observed in the presence of bicuculline, a $GABA_A$ receptor antagonist, in all cases (unpublished data). These results suggest that the abnormal excitability observed in μ3B$^{-/-}$ΔNeo mice is due to the impairment in GABAergic inhibition in the TA pathway.

Discussion

There are two distinct pathways for synaptic vesicle formation: endocytosis or recycling from the plasma membrane and budding from the endosomal membrane (Hannah et al., 1999; Murthy and De Camilli, 2003). Although the AP-2–dependent recycling pathway is believed to be the major pathway for the generation of synaptic vesicles (Murthy and De Camilli, 2003), the importance of the endosomal pathway for the biogenesis of synaptic vesicles has been unclear. Although we and others have shown the implication of AP-3B in the biogenesis of synaptic vesicles from endosomes in vitro (Faundez et al., 1998; Blumstein et al., 2001), its physiological role has remained uncertain. Here, we demonstrated that hippocampal inhibitory synaptic vesicles in μ3B-deficient mice show defects in both morphology and function, indicating that AP-3B plays an essential role in normal synaptic function in vivo by regulating the biogenesis of at least a subset of synaptic vesicles. Thus, this work is the first to demonstrate that, in addition to AP-2–dependent recycling pathway, the AP-3B–dependent synaptic vesicle formation is also of physiological importance in the central nervous system.

μ3B$^{-/-}$ΔNeo mice were observed to suffer from spontaneous recurrent epileptic seizures. They were also more susceptible to drug-induced seizures than their wild-type counterpart. The kindling procedure revealed that μ3B$^{-/-}$ΔNeo mice rapidly reached class 5, or generalized seizure. Judging from the observations of the seizure phenotype, however, we surmise that the generalized seizure in μ3B$^{-/-}$ΔNeo mice evoked by kindling stimulation is due to intrinsic epileptogenesis rather than induction by the kindling. It is considered that the suppression by inhibitory neurons of the propagation of kindling–stimulation-induced hyperexcitability prevents the development of behavioral seizures in wild-type mice at the early stages of kindling (Sato et al., 1990). Therefore, the generalized seizure in μ3B$^{-/-}$ΔNeo mice induced at the early stages of kindling further suggests a disorder in the inhibitory neurons in the mice.

AP-3A deficiency in mammals, such as HPS patients and *pearl* mice, was reported to result in the dysfunction of lysosomes and lysosome-related organelles (Dell'Angelica et al., 1999; Swank et al., 2000). In contrast to AP-3A, however, the function of AP-3B has remained unknown. *Mocha* mice lacking both AP-3A and AP-3B show neurological phenotypes including abnormal electrocorticogram and inner ear disorders such as deafness and balance problem, in addition to the phenotype seen in AP-3A deficiency (Noebels and Sidman, 1989; Kantheti et al., 1998). Therefore, the neurological disorder observed in *mocha* mice has been predicted to be due to the AP-3B deficiency. Contrary to the prediction, however, μ3B$^{-/-}$ΔNeo mice exhibited neither deafness nor balance problem. The inner ear disorder has been attributed to an insufficiency of heavy metals such as zinc and/or manganese (Rolfsen and Erway, 1984). Kantheti et al. (1998) reported the lack of zinc as well as ZnT-3, a zinc transporter localized in synaptic vesicles, in the brain of *mocha* mice. By contrast, we observed neither any apparent differences in zinc staining nor the immunolocalization of ZnT-3 in the hippocampus of μ3B$^{-/-}$ΔNeo mice as well as *pearl* mice, consistent with the lack of inner ear symptoms in these mice (unpublished data). These observations suggest that the inner ear phenotype as well as the mislocalization of ZnT-3 only appears when both AP-3A and AP-3B are deficient in *mocha* mice.

Functional as well as ultrastructural analyses corroborate the impaired inhibitory synaptic transmission in the absence of μ3B. The K^+-evoked release of GABA was decreased significantly in μ3B$^{-/-}$ΔNeo mice compared with wild-type mice, whereas that of glutamate was not affected. Electrophysiological experiments demonstrated that,

Published October 18, 2004

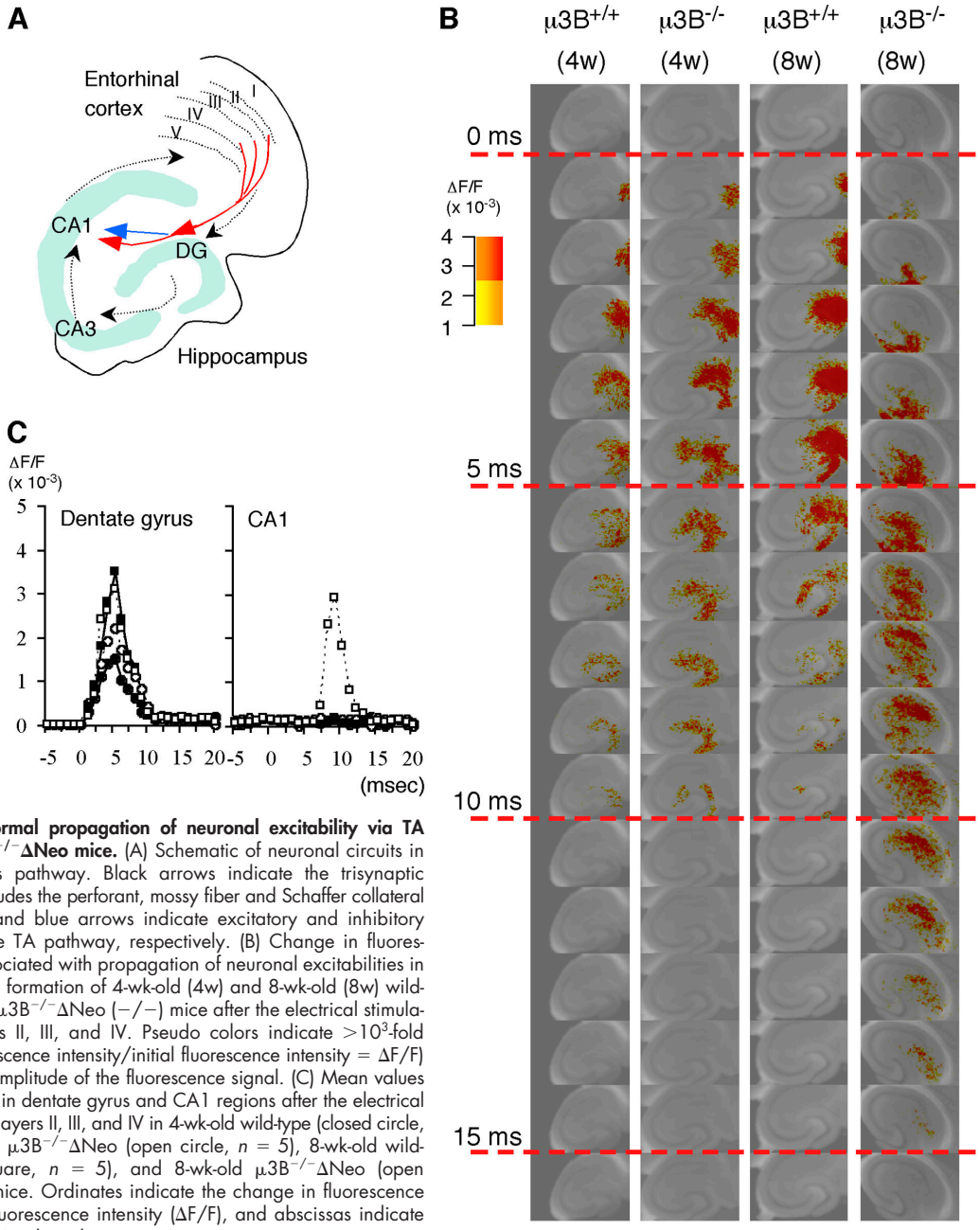

Figure 6. **Abnormal propagation of neuronal excitability via TA pathway in μ3B$^{-/-}$ΔNeo mice.** (A) Schematic of neuronal circuits in EC–hippocampus pathway. Black arrows indicate the trisynaptic pathway that includes the perforant, mossy fiber and Schaffer collateral pathways. Red and blue arrows indicate excitatory and inhibitory projections in the TA pathway, respectively. (B) Change in fluorescence signal associated with propagation of neuronal excitabilities in EC–hippocampal formation of 4-wk-old (4w) and 8-wk-old (8w) wild-type (+/+) and μ3B$^{-/-}$ΔNeo (−/−) mice after the electrical stimulation of EC layers II, III, and IV. Pseudo colors indicate >10^3-fold (change in fluorescence intensity/initial fluorescence intensity = ΔF/F) elevation in the amplitude of the fluorescence signal. (C) Mean values of optical signals in dentate gyrus and CA1 regions after the electrical stimulation of EC layers II, III, and IV in 4-wk-old wild-type (closed circle, n = 5), 4-wk-old μ3B$^{-/-}$ΔNeo (open circle, n = 5), 8-wk-old wild-type (closed square, n = 5), and 8-wk-old μ3B$^{-/-}$ΔNeo (open square, n = 4) mice. Ordinates indicate the change in fluorescence intensity/initial fluorescence intensity (ΔF/F), and abscissas indicate time after stimulation (msec).

in μ3B$^{-/-}$ΔNeo mice, LTP was induced under the condition that synaptic potentiation was not induced because of the GABAergic synaptic inhibition in wild-type mice. Furthermore, optical recording experiments demonstrated that the neuronal excitability in EC propagated to the CA1 region in the μ3B-deficient condition (8-wk-old μ3B$^{-/-}$ΔNeo mice), which was not observed in the normal condition. The TA pathway can enhance via direct excitatory projection, or suppress via indirect GABAergic interneuron-associated projection, the excitability of CA1 pyramidal cells (Heinemann et al., 2000; Remondes and Schuman, 2002). Together, the results suggest the impairment of GABAergic synaptic inhibition and are consistent with the impairment of GABA release in μ3B$^{-/-}$ΔNeo mice.

Considering that AP-3B is likely expressed in virtually all neurons, the apparent difference in phenotype between excitatory and inhibitory neurons is not fully understood. Similar phenotypic differences between excitatory and inhibitory neurons were observed in several mice deficient in synaptic vesicle proteins (Augustin et al., 1999; Terada et al., 1999; Schoch et al., 2002). Excitatory and inhibitory neurons may exhibit different dependences on these molecules as well as AP-3B to exert their functions. It is also possible that an inhibitory-synapse–specific cargo protein of AP-3B may be responsible for the difference. We surmise that VGAT is an obvious cargo candidate. The amount of VGAT was decreased in the hippocampus of μ3B$^{-/-}$ΔNeo mice. It has been shown that *unc-47*, a VGAT mutant of *C. elegans,* displays an impairment in

Published October 18, 2004

GABAergic neurotransmission (McIntire et al., 1997). Therefore, it is conceivable that the impairment of GABAergic synaptic function in μ3B$^{-/-}$ΔNeo mice is, at least in part, due to the reduction of the hippocampal VGAT proteins. Notably, we have identified a potential di-leucine signal, one of the well-characterized sorting signals recognized by AP complexes (Bonifacino and Traub, 2003), in the cytoplasmic tail of VGAT (unpublished data). Thus, AP-3B may play a role in the inclusion of VGAT into synaptic vesicles. However, no reduction of VGAT was detected in the whole brain of μ3B$^{-/-}$ΔNeo mice. One of the possible explanations is that the reduction was apparent in the μ3B$^{-/-}$ΔNeo hippocampus, where the expression level of the μ3B is among the highest and more neurons may depend on μ3B for the targeting of VGAT to synaptic vesicles. Further studies are conducted to address this issue.

In conclusion, the present work has demonstrated the critical role of AP-3B in functional synaptic transmission, particularly the inhibitory one. μ3B deficiency caused an impairment of GABA release possibly because of the reduction of VGAT, which is reflected by the decreased threshold of LTP induction and the abnormal propagation of neuronal excitability in the hippocampus. As a result, μ3B-deficient mice suffered from recurrent epileptic seizure. μ3B$^{-/-}$ΔNeo mice may serve as a novel animal model of epilepsy, one of the most common neurological disorders, to benefit epileptic patients in the future.

Materials and methods

Animals

All animal experiments were performed in accordance with the guidelines for the care and use of laboratory animals in RIKEN, Kanazawa University, Hirosaki University, Kobe University, Chiba University, Hokkaido University, and University of Tokyo.

Generation of μ3B-deficient mice

A genomic DNA clone containing the μ3B gene was isolated from a mouse 129SV/J genomic library (Stratagene). The targeting vector consisted of a 3-kb EcoRI genomic fragment, EGFP cDNA (CLONTECH Laboratories, Inc.), the Neo gene flanked with two loxP sites (H. Gu, Columbia University, New York, NY; Nishimura et al., 2002) at both ends, a 1.5-kb SalI–BamHI genomic fragment, and the HSV-tk gene in pBluescript II SK(+) (Stratagene), as depicted in Fig. 1. EGFP cDNA was placed in frame immediately after the start codon of the μ3B gene so that EGFP was transcribed under the control of μ3B promoter activity. The targeting vector was transfected into ES cells by electroporation. Homologous recombination was confirmed by Southern blotting using both probes S (a PCR product) and L (an EcoRI–SspI 0.5-kb fragment). μ3B$^{-/-}$ mice were generated essentially as described previously (Ohno et al., 1993). We obtained μ3B$^{-/-}$ mice lacking the Neo gene (μ3B$^{-/-}$ΔNeo mice) by crossing them with Cre-transgenic mice (Sakai and Miyazaki, 1997). Deletion of the Neo gene was confirmed by Southern blotting using both probe L (Fig. 1 A) and Neo probe (not depicted). We further backcrossed the μ3B$^{-/-}$ΔNeo mice with C57BL/6 mice to at least seven generations to establish μ3B$^{-/-}$ΔNeo mice with the C57BL/6 background. RT-PCR was performed using sense (5′-atgctggacaatgggttcccc-3′) and antisense (5′-aattgtagggttctcatcggg-3′) primers for μ3B, and sense (5′-caccggcctctccaccatg-3′) and antisense (5′-gtgttctgctggtagtggtcg-3′) primers for EGFP. All experiments were conducted using littermate or age-matched C57BL/6 mice as control.

Immunoblotting

Whole brains or hippocampi from mice with both genotypes were homogenized in lysis buffer containing 320 mM sucrose and 10 mM Hepes, pH 7.4, with protease inhibitors (Roche Molecular Biochemicals). Synaptosomal and LP2 fraction was prepared as described previously (Huttner et al., 1983). The lysates were subjected to SDS-PAGE and immunoblotting using the following antibodies: anti–α adaptin (AP.6; American Type Culture Collection), anti-synaptotagmin and anti-VAMP2 (M. Takahashi, Kitazato University, Sagamihara, Japan), anti-synaptophysin (SY38; PROGEN), anti–rabphilin-3A and β3B (BD Transduction Laboratory), anti-μ3 (J.S. Bonifacino, National Institutes of Health, Bethesda, MD), anti-Rab3A (Y. Takai, Osaka University, Suita, Japan), anti-GAPDH (CHEMICON International, Inc.), anti-VGLUT1 and anti-VGLUT2 (R.H. Edwards, University of California San Francisco, San Francisco, CA), anti-ZnT3 antibody (T. Palmiter, University of Washington, Seattle, WA), and anti-VGAT antibody (Miyazaki et al., 2003). Western blots were visualized with an ECL system (Super Signal; Pierce Chemical Co.). Chemiluminescence signals were detected by LAS-1000 plus (Fuji Photo Film) and quantified using Image Gause Software (Fuji Photo Film).

Electrocorticogram

Mice were anesthetized with pentobarbital (40 mg/kg, i.p.). Bipolar silver ball electrodes (diameter, 1.0 mm; distance, 3.5 mm) were stereotaxically implanted onto the epidural surface of the left primary motor and left primary somatosensory cortices according to the stereotaxic coordinates of Franklin and Paxinos (2001): 1.18 mm anterior to the bregma and 1.2 mm lateral to the midline, and 2.06 mm posterior to the bregma and 3.0 mm lateral to the midline, respectively. After convalescence for at least 2 wk, electrocorticogram was recorded with a continuous video-EEG monitoring system for freely moving mice.

Pharmacological analysis of seizure susceptibility

The experiment was performed essentially as described previously (Tecott et al., 1995). In brief, PTZ (Sigma-Aldrich) was infused into the tail vein of wild-type (4 wk old, $n = 6$; 8 wk old, $n = 5$) or μ3B$^{-/-}$ΔNeo (4 wk old, $n = 4$; 8 wk old, $n = 5$) mice at a constant rate (1.5 mg/min) and the time required by the animals to go through four stages as judged by their behavior was measured in a blind fashion. The stages are as follows: stage I, no movement; stage II, twitches of head and body; stage III, tonic–clonic convulsion; and stage IV, extension and death.

Electrical kindling

Before the surgical procedures, the mice were anesthetized with pentobarbital (40 mg/kg, i.p.). A bipolar stimulation-recording electrode made of stainless steel was stereotaxically implanted into the left basolateral nucleus of the amygdala according to the stereotaxic coordinates of Franklin and Paxinos (2001): 1.94 mm posterior from the bregma, 2.9 mm lateral from the midline and 4.2 mm below the dura mater.

After a recovery period of 10 d, the mice were exposed to kindling stimulation of the left amygdala once daily, consisting of 2 s, 50 Hz biphasic square pulses at the intensity of the afterdischarge threshold. The development of behavioral seizures was classified according to the criteria of Racine (1972).

Morphological studies

Mice from both genotypes were anesthetized with pentobarbital sodium (50 mg/kg) and transcardially perfused with 4% PFA in 0.1 M phosphate buffer, pH 7.4, at 2, 4, 6, 8, and 16 wk old ($n = 3$, respectively). 4-μm-thick, paraffin-embedded sections were prepared and stained with hematoxylin and eosin and by the Klüver-Barrera method.

For immunohistochemistry, 50-μm-thick vibratome sections were immunostained using the avidin–biotin–peroxidase complex method with a Vectastain avidin–biotin–peroxidase complex kit (Vector Laboratories). The sections were incubated with rabbit anti–mouse GAD67 antibody (1:100; Yamada et al., 2001), rabbit anti-VGAT antibody (1:1,000; Miyazaki et al., 2003) and rabbit anti-GFAP antibody (1:500; DakoCytomation). The reaction was visualized with 0.02% 3,-3′-DAB tetrachloride and 0.005% H_2O_2 in 0.05 M Tris-HCl buffer, pH 7.6, for 10 min at RT.

For EM, the brains were fixed with 2.5% glutaraldehyde in 0.1 M phosphate buffer, pH 7.4, and 50-μm-thick vibratome sections were cut from the hippocampus. Inhibitory synaptic inputs to the hippocampus are known to converge onto the perisomatic region as well as the basal and apical dendrites of pyramidal cells (Freund and Buzsaki, 1996). Virtually all the synapses on pyramidal cell somata contained pleomorphic vesicles associated with symmetric membrane differentiations, characteristic of inhibitory synapses (Beaulieu and Colonnier, 1985; Freund and Buzsaki, 1996). In addition, nerve terminals immunoreactive for VGAT, a marker for inhibitory neurons (McIntire et al., 1997; Chaudhry et al., 1998), were numerous in the perisomatic region of the CA1 pyramidal cells. Based on these observations, the axon terminals containing pleomorphic vesicles and making symmetric synaptic contact with the pyramidal cell somata were considered to be inhibitory GABAergic terminals. Electron micrographs (×30,000) of asymmetric synaptic terminals in the stratum

Published October 18, 2004

lacunosum-moleculare (excitatory terminals) and symmetric synaptic terminals that contact with pyramidal cell somata (inhibitory terminals) of the CA1 were taken from random positions. Morphometric analysis was performed on enlarged prints (×45,000). The synaptic boutons and vesicles were digitized using a Macintosh personal computer with a flat head scanner and an interactive pen display at a final magnification of 90,000. NIH Image 1.62 software was used to calculate the areas of synaptic boutons and the numbers and diameters of the synaptic vesicles. All morphometric analyses were performed without knowledge of the genotype by coding specimens.

Measurement of neurotransmitter level

The determination of neurotransmitter release from the hippocampal minislice was performed according to previous studies (Zhu et al., 2000; Okada et al., 2003). The levels of glutamate and GABA were determined by HPLC with fluorescence detection (Zhu et al., 2000; Okada et al., 2001). The excitation and emission fluorescence wavelengths were 340 and 445 nm, respectively. The mobile phase was 0.1 M phosphate buffer, pH 6.0, containing 20% methanol and the flow rate was 300 l/min (Zhu et al., 2000; Okada et al., 2003).

Electrophysiological analysis

Mutant and their littermate wild-type mice (male; 7–14 wk old) were deeply anesthetized with halothane and decapitated, and then the brains were removed. Hippocampal slices (400 μm thick) were cut with a vibratome tissue slicer and placed in a humidified interface-type holding chamber for at least 1 h. A single slice was then transferred to the recording chamber and submerged in a continuously perfusing medium that had been saturated with 95% O_2/5%CO_2. The medium contained 119 mM NaCl, 2.5 mM KCl, 1.3 mM $MgSO_4$, 2.5 mM $CaCl_2$, 1.0 mM NaH_2PO_4, 26.2 mM $NaHCO_3$, and 11 mM glucose. All experiments were conducted at 25–26°C. Field-potential recordings were made using a glass electrode (3 M NaCl) placed in the stratum radiatum of the CA1 region. An amplifier (model Axopatch 1D; Axon Instruments) was used and the signal was filtered at 1 kHz. Responses were digitized at 10 kHz, stored in a personal computer and analyzed using pClamp 8.1 (Axon Instruments). To evoke excitatory synaptic responses, a bipolar tungsten stimulating electrode was placed in the stratum radiatum, and Schaffer collateral/commissural fibers were stimulated at 0.1 Hz. All experiments were performed in a blind fashion. The data are expressed as means ± SEM. The *t* test was used for determining whether there was a significant difference ($P < 0.05$) in the mean between two sets of data.

Optical recording

The procedure for the preparation of brain slices (300 μm) including EC and ventral hippocampus was based on the experimental procedures described in a previous work (Okada et al., 2003). After stabilization, 100 mM di-4-ANEPPS (Molecular Probes), dissolved in 2.7% ethanol and 0.13% Cremophor EL, was added to the incubation medium for 30 min to stain the brain slice. The final concentration of di-4-ANEPPS in the incubation medium was 100 μM.

The MED probe was composed of transparent materials except the electrodes, thereby allowing the localization of the electrodes in the slice under a microscope. After staining, each slice was positioned on a MED probe (MED-P5155; Alpha MED Sciences Co.) such that the array of electrodes was consistent with regard to layers II, III, and IV. The imaging system used a high-speed fluorescence CCD camera (MiCAM01; BrainVision) and a fluorescence microscope (THT-aIII; BrainVision) consisting of an objective lens (PLANAPO × 1; Leica), a projection lens (PLANAPO × 1.6; Leica), a dichroic mirror (575 nm), and absorption (530 nm) and excitation (590 nm) filters (Tominaga et al., 2001; Okada et al., 2004).

During optical recording, the MED probe was superfused with artificial cerebrospinal fluid (in mM: NaCl 124, KCl 5, $MgSO_4$ 1.3, Na_2HPO_4 1.25, $CaCl_2$ 2.6, $NaHCO_3$ 22, glucose 10) bubbled with 95% O_2 and 5% CO_2 and maintained continuously at 35°C (Zhu et al., 2000; Okada et al., 2003). EC layers II, III, and IV were stimulated by three electrodes simultaneously at 5 s intervals. The stimulation intensity was adjusted to obtain a submaximal evoked field potential (100 μA). Each stimulus consisted of bipolar constant current pulses of 100 μsec duration. Stimulation patterns were designed using data acquisition software (Panasonic: MED conductor) and delivered through an isolator (BSI-2; Alpha MED Sciences Co.). These procedures of electrical stimulation were controlled using a computer running on Windows NT.

Online supplemental material

Fig. S1 depicts localization of synaptic vesicle proteins in the hippocampus of wild-type and μ3B$^{-/-}$ΔNeo mice. Video 1 shows spontaneous seizure of μ3B$^{-/-}$ΔNeo mice. Online supplemental material is available at http://www.jcb.org/cgi/content/full/jcb.200405032/DC1.

We would like to thank Dr. T. Shirasawa for analysis of knockout mice; Drs. H. Kakuda, K. Saijo, K. Arase, and H. Koseki for help in the establishment of ES cells; Drs. J. S. Bonifacino, Y. Takai, H. Gu, M. Takahashi, T. Palmiter, and R.H. Edwards for generously providing the reagents; Ms. M. Sakuma, R. Shiina, M. Matsumoto, N. Nakatsu, T, Imamura, M. Kakiuchi, M. Watanabe, and N. Shioda for expert technical assistance; Drs. N. Nakamura, H. Takatsu, and K. Hase for critical reading of the manuscript; and Ms. H. Yamaguchi, Y. Kurihara, and Y. Takase for secretarial assistance.

This work was supported by Grants-in-Aid for Young Scientists (B) (to F. Nakatsu), Scientific Research (to H. Ohno, H. Kamiya, T. Manabe, and F. Mori), Scientific Research in Priority Areas (to H. Ohno), Protein 3000 Project (to H. Ohno) and Special Coordination Funds for the Promotion of Science and Technology (to T. Manabe) from the Ministry of Education, Culture, Sports, Science and Technology of Japan, RISTEX, JST (Japan Science and Technology Agency; to T. Manabe), the Uehara Memorial Foundation (to H. Ohno), the Naito Foundation (to H. Ohno and T. Manabe), the Sumitomo Foundation (to T. Manabe), and the Terumo Life Science Foundation (to T. Manabe). We declare that we have no competing financial interests.

Submitted: 6 May 2004
Accepted: 24 August 2004

References

Augustin, I., C. Rosenmund, T.C. Sudhof, and N. Brose. 1999. Munc13-1 is essential for fusion competence of glutamatergic synaptic vesicles. *Nature.* 400:457–461.

Beaulieu, C., and M. Colonnier. 1985. A laminar analysis of the number of round-asymmetrical and flat-symmetrical synapses on spines, dendritic trunks, and cell bodies in area 17 of the cat. *J. Comp. Neurol.* 231:180–189.

Blumstein, J., V. Faundez, F. Nakatsu, T. Saito, H. Ohno, and R.B. Kelly. 2001. The neuronal form of adaptor protein-3 is required for synaptic vesicle formation from endosomes. *J. Neurosci.* 21:8034–8042.

Boehm, M., and J.S. Bonifacino. 2001. Adaptins: the final recount. *Mol. Biol. Cell.* 12:2907–2920.

Bonifacino, J.S., and E.C. Dell'Angelica. 1999. Molecular bases for the recognition of tyrosine-based sorting signals. *J. Cell Biol.* 145:923–926.

Bonifacino, J.S., and L.M. Traub. 2003. Signals for sorting of transmembrane proteins to endosomes and lysosomes. *Annu. Rev. Biochem.* 72:395–447.

Chaudhry, F.A., R.J. Reimer, E.E. Bellocchio, N.C. Danbolt, K.K. Osen, R.H. Edwards, and J. Storm-Mathisen. 1998. The vesicular GABA transporter, VGAT, localizes to synaptic vesicles in sets of glycinergic as well as GABAergic neurons. *J. Neurosci.* 18:9733–9750.

Dell'Angelica, E.C., V. Shotelersuk, R.C. Aguilar, W.A. Gahl, and J.S. Bonifacino. 1999. Altered trafficking of lysosomal proteins in Hermansky-Pudlak syndrome due to mutations in the beta 3A subunit of the AP-3 adaptor. *Mol. Cell.* 3:11–21.

Faundez, V., J.T. Horng, and R.B. Kelly. 1998. A function for the AP3 coat complex in synaptic vesicle formation from endosomes. *Cell.* 93:423–432.

Feng, L., A.B. Seymour, S. Jiang, A. To, A.A. Peden, E.K. Novak, L. Zhen, M.E. Rusiniak, E.M. Eicher, M.S. Robinson, et al. 1999. The beta3A subunit gene (Ap3b1) of the AP-3 adaptor complex is altered in the mouse hypopigmentation mutant pearl, a model for Hermansky-Pudlak syndrome and night blindness. *Hum. Mol. Genet.* 8:323–330.

Franklin, K.B., and Paxinos, G. 2001. The Mouse Brain in Stereotaxic Coordinates. Academic Press, San Diego. 188 pp.

Fremeau, R.T., Jr., M.D. Troyer, I. Pahner, G.O. Nygaard, C.H. Tran, R.J. Reimer, E.E. Bellocchio, D. Fortin, J. Storm-Mathisen, and R.H. Edwards. 2001. The expression of vesicular glutamate transporters defines two classes of excitatory synapse. *Neuron.* 31:247–260.

Freund, T.F., and G. Buzsaki. 1996. Interneurons of the hippocampus. *Hippocampus.* 6:347–470.

Gasnier, B. 2000. The loading of neurotransmitters into synaptic vesicles. *Biochimie.* 82:327–337.

Goddard, G.V. 1967. Development of epileptic seizures through brain stimulation at low intensity. *Nature.* 214:1020–1021.

Hannah, M.J., A.A. Schmidt, and W.B. Huttner. 1999. Synaptic vesicle biogenesis. *Annu. Rev. Cell Dev. Biol.* 15:733–798.

Heinemann, U., D. Schmitz, C. Eder, and T. Gloveli. 2000. Properties of entorhinal cortex projection cells to the hippocampal formation. *Ann. NY Acad. Sci.* 911:112–126.

Hirst, J., and M.S. Robinson. 1998. Clathrin and adaptors. *Biochim. Biophys.*

Acta. 1404:173–193.

Huttner, W.B., W. Schiebler, P. Greengard, and P. De Camilli. 1983. Synapsin I (protein I), a nerve terminal-specific phosphoprotein. III. Its association with synaptic vesicles studied in a highly purified synaptic vesicle preparation. *J. Cell Biol.* 96:1374–1388.

Kantheti, P., X. Qiao, M.E. Diaz, A.A. Peden, G.E. Meyer, S.L. Carskadon, D. Kapfhamer, D. Sufalko, M.S. Robinson, J.L. Noebels, and M. Burmeister. 1998. Mutation in AP-3 delta in the mocha mouse links endosomal transport to storage deficiency in platelets, melanosomes, and synaptic vesicles. *Neuron.* 21:111–122.

Kirchhausen, T., J.S. Bonifacino, and H. Riezman. 1997. Linking cargo to vesicle formation: receptor tail interactions with coat proteins. *Curr. Opin. Cell Biol.* 9:488–495.

McIntire, S.L., R.J. Reimer, K. Schuske, R.H. Edwards, and E.M. Jorgensen. 1997. Identification and characterization of the vesicular GABA transporter. *Nature.* 389:870–876.

Miyazaki, T., M. Fukaya, H. Shimizu, and M. Watanabe. 2003. Subtype switching of vesicular glutamate transporters at parallel fibre-Purkinje cell synapses in developing mouse cerebellum. *Eur. J. Neurosci.* 17:2563–2572.

Murthy, V.N., and P. De Camilli. 2003. Cell biology of the presynaptic terminal. *Annu. Rev. Neurosci.* 26:701–728.

Nakatsu, F., and H. Ohno. 2003. Adaptor protein complexes as the key regulators of protein sorting in the post-Golgi network. *Cell Struct. Funct.* 28: 419–429.

Newman, L.S., M.O. McKeever, H.J. Okano, and R.B. Darnell. 1995. Beta-NAP, a cerebellar degeneration antigen, is a neuron-specific vesicle coat protein. *Cell.* 82:773–783.

Nishimura, K., F. Nakatsu, K. Kashiwagi, H. Ohno, T. Saito, and K. Igarashi. 2002. Essential role of S-adenosylmethionine decarboxylase in mouse embryonic development. *Genes Cells.* 7:41–47.

Noebels, J.L., and R.L. Sidman. 1989. Persistent hypersynchronization of neocortical neurons in the mocha mutant of mouse. *J. Neurogenet.* 6:53–56.

Odorizzi, G., C.R. Cowles, and S.D. Emr. 1998. The AP-3 complex: a coat of many colours. *Trends Cell Biol.* 8:282–288.

Ohno, H., T. Aoe, S. Taki, D. Kitamura, Y. Ishida, K. Rajewsky, and T. Saito. 1993. Developmental and functional impairment of T cells in mice lacking CD3 zeta chains. *EMBO J.* 12:4357–4366.

Ohno, H., J. Stewart, M.C. Fournier, H. Bosshart, I. Rhee, S. Miyatake, T. Saito, A. Gallusser, T. Kirchhausen, and J.S. Bonifacino. 1995. Interaction of tyrosine-based sorting signals with clathrin-associated proteins. *Science.* 269:1872–1875.

Okada, M., D.J. Nutt, T. Murakami, G. Zhu, A. Kamata, Y. Kawata, and S. Kaneko. 2001. Adenosine receptor subtypes modulate two major functional pathways for hippocampal serotonin release. *J. Neurosci.* 21: 628–640.

Okada, M., G. Zhu, S. Hirose, K.I. Ito, T. Murakami, M. Wakui, and S. Kaneko. 2003. Age-dependent modulation of hippocampal excitability by KCNQ-channels. *Epilepsy Res.* 53:81–94.

Okada, M., G. Zhu, S. Yoshida, S. Hirose, and S. Kaneko. 2004. Protein kinase associated with gating and closing transmission mechanism in temporoammonic pathway. *Neuropharmacology.* 47:485–504.

Olson, E.N., H.H. Arnold, P.W. Rigby, and B.J. Wold. 1996. Know your neighbors: three phenotypes in null mutants of the myogenic bHLH gene MRF4. *Cell.* 85:1–4.

Pevsner, J., W. Volknandt, B.R. Wong, and R.H. Scheller. 1994. Two rat homologs of clathrin-associated adaptor proteins. *Gene.* 146:279–283.

Racine, R.J. 1972. Modification of seizure activity by electrical stimulation. II. Motor seizure. *Electroencephalogr. Clin. Neurophysiol.* 32:281–294.

Reimer, R.J., E.A. Fon, and R.H. Edwards. 1998. Vesicular neurotransmitter transport and the presynaptic regulation of quantal size. *Curr. Opin. Neurobiol.* 8:405–412.

Remondes, M., and E.M. Schuman. 2002. Direct cortical input modulates plasticity and spiking in CA1 pyramidal neurons. *Nature.* 416:736–740.

Rolfsen, R.M., and L.C. Erway. 1984. Trace metals and otolith defects in mocha mice. *J. Hered.* 75:159–162.

Sakai, K., and J. Miyazaki. 1997. A transgenic mouse line that retains Cre recombinase activity in mature oocytes irrespective of the cre transgene transmission. *Biochem. Biophys. Res. Commun.* 237:318–324.

Sato, M., R.J. Racine, and D.C. McIntyre. 1990. Kindling: basic mechanisms and clinical validity. *Electroencephalogr. Clin. Neurophysiol.* 76:459–472.

Schoch, S., P.E. Castillo, T. Jo, K. Mukherjee, M. Geppert, Y. Wang, F. Schmitz, R.C. Malenka, and T.C. Sudhof. 2002. RIM1alpha forms a protein scaffold for regulating neurotransmitter release at the active zone. *Nature.* 415:321–326.

Swank, R.T., E.K. Novak, M.P. McGarry, Y. Zhang, W. Li, Q. Zhang, and L. Feng. 2000. Abnormal vesicular trafficking in mouse models of Hermansky-Pudlak syndrome. *Pigment Cell Res.* 13:59–67.

Tecott, L.H., L.M. Sun, S.F. Akana, A.M. Strack, D.H. Lowenstein, M.F. Dallman, and D. Julius. 1995. Eating disorder and epilepsy in mice lacking 5-HT2c serotonin receptors. *Nature.* 374:542–546.

Terada, S., T. Tsujimoto, Y. Takei, T. Takahashi, and N. Hirokawa. 1999. Impairment of inhibitory synaptic transmission in mice lacking synapsin I. *J. Cell Biol.* 145:1039–1048.

Tominaga, T., Y. Tominaga, and M. Ichikawa. 2001. Simultaneous multi-site recordings of neural activity with an inline multi-electrode array and optical measurement in rat hippocampal slices. *Pflugers Arch.* 443:317–322.

Wigstrom, H., and B. Gustafsson. 1983. Facilitated induction of hippocampal long-lasting potentiation during blockade of inhibition. *Nature.* 301: 603–604.

Yamada, K., M. Fukaya, H. Shimizu, K. Sakimura, and M. Watanabe. 2001. NMDA receptor subunits GluRepsilon1, GluRepsilon3 and GluRzeta1 are enriched at the mossy fibre-granule cell synapse in the adult mouse cerebellum. *Eur. J. Neurosci.* 13:2025–2036.

Zhu, G., M. Okada, T. Murakami, A. Kamata, Y. Kawata, K. Wada, and S. Kaneko. 2000. Dysfunction of M-channel enhances propagation of neuronal excitability in rat hippocampus monitored by multielectrode dish and microdialysis systems. *Neurosci. Lett.* 294:53–57.